CAD Models of Lumped Elements on GaAs up to 18 GHz

EWALD PETTENPAUL, HARTMUT KAPUSTA, ANDREAS WEISGERBER, HEINRICH MAMPE, JÜRGEN LUGINSLAND, AND INGO WOLFF, SENIOR MEMBER, IEEE

Abstract — **Improved models for integrable lumped-element straight-line single-loop, and spiral inductors, as well as for interdigitated and MIM capacitors, have been derived using numerical solutions of the inductance integral, basic microstrip theory, and network analysis. The broad experimental verification shows good agreement between models and experiments, with deviations of 5 to 10 percent up to 18 GHz. Besides the useful value and frequency range, losses of the lumped elements are presented.**

I. Introduction

A FLEXIBLE CIRCUIT design philosophy for GaAs MMIC's must include both lumped elements with dimensions smaller than 0.1 wavelength, and distributed elements. The choice of lumped or distributed elements depends mainly on the type of the MMIC, the acceptable chip size and necessary range of values, the acceptable losses or Q factors, and the operating frequency. Lumped elements are considered as very attractive structures for the realization of MMIC's with respect to a considerable size reduction.

The use of lumped rather than distributed elements for the realization of hybrid integrated microwave amplifiers up to the S-band has been described intensively in the litarature (e.g. [1]). For the design of these circuits in most cases approximate dc current formulas have been used with sufficient success.

In 1943 Terman [2] published an expression for the inductance of a thin metallic straight line which was improved by Caulton *et al.* [1], who additionally considered the influence of the metallization thickness approximately. Wheeler [4] already in 1928 presented a frequently applied approximating formula for the inductance of a circular spiral inductor, which also showed good agreement with RF measurements at low microwave frequencies. This formula has been intensively used for the design of microwave lumped circuits [3], [5], [6], [22].

A first theory for the interdigitated capacitor was published by Alley [38], but his theory already showed that this complicated structure cannot be described exactly by simple formulas. Nevertheless Joshi *et al.* [9] presented approximating formulas for the interdigitated capacitor which are accurate enough for a first design step.

Between 1977 and 1979, Pengelly *et al.* [11] presented the first extensive results on different lumped elements on GaAs, with special emphasis on Q-factor examination. They measured Q factors near 120 for single-loop inductors and interdigitated capacitors.

This work reports on advanced models for different lumped-element structures: straight-line inductors, single-loop and spiral inductors, and overlay (MIM) and interdigitated capacitors. A schematic representation of the structures is shown in Fig. 1. The models used allow the derivation of equivalent circuit elements including all important parasitics by the application of state-of-the-art electromagnetic field theory and microstrip theory in order to determine accurate element values and losses.

The experimental verification of all models with extensive scaling investigations of the structures and improved test procedures is another main part of this work. As a result, standard design rules for the layout of the elements can be derived which consider the useful value range, frequency range, losses, miniaturization, and some other aspects.

II. Model Description

Only a short overview on the methods applied to model the lumped elements can be given here. As a general result it is found that modeling of lumped elements is such a complicated matter that normally a component cannot be described by just one simple formula if all parasitic influences are to be considered. Therefore generally the model for a lumped element consists of a computer program which brings together many formulas and theoretical calculations for describing the circuit parameters (R, L, C) in dependence on the geometrical and electrical parameters and the frequency. Because the computer programs are to be used in computer-aided circuit analysis, in any case the solution is used which leads to the smallest computing time and acceptable accuracy.

A. The Conductor Losses

Lumped elements in MMIC's may have line widths between 5 μm and 20 μm and a metallization thickness between 2 μm and 5 μm. This means first that the line

Manuscript received April 25, 1987; revised October 7, 1987. This work was supported in part by the European Community ESPRIT Research Program under Project 255.

E. Pettenpaul, H. Kapusta, A. Weisgerber, H. Mampe, and J. Luginsland are with Siemens AG, Components Group, D-8000 Munich, West Germany.

I. Wolff is with the Department of Electrical Engineering and Sonderforschungsbereich 254, University of Duisburg, D-4100 Duisburg, West Germany.

IEEE Log Number 8718473

0018-9480/88/0200-0294$01.00 ©1988 IEEE

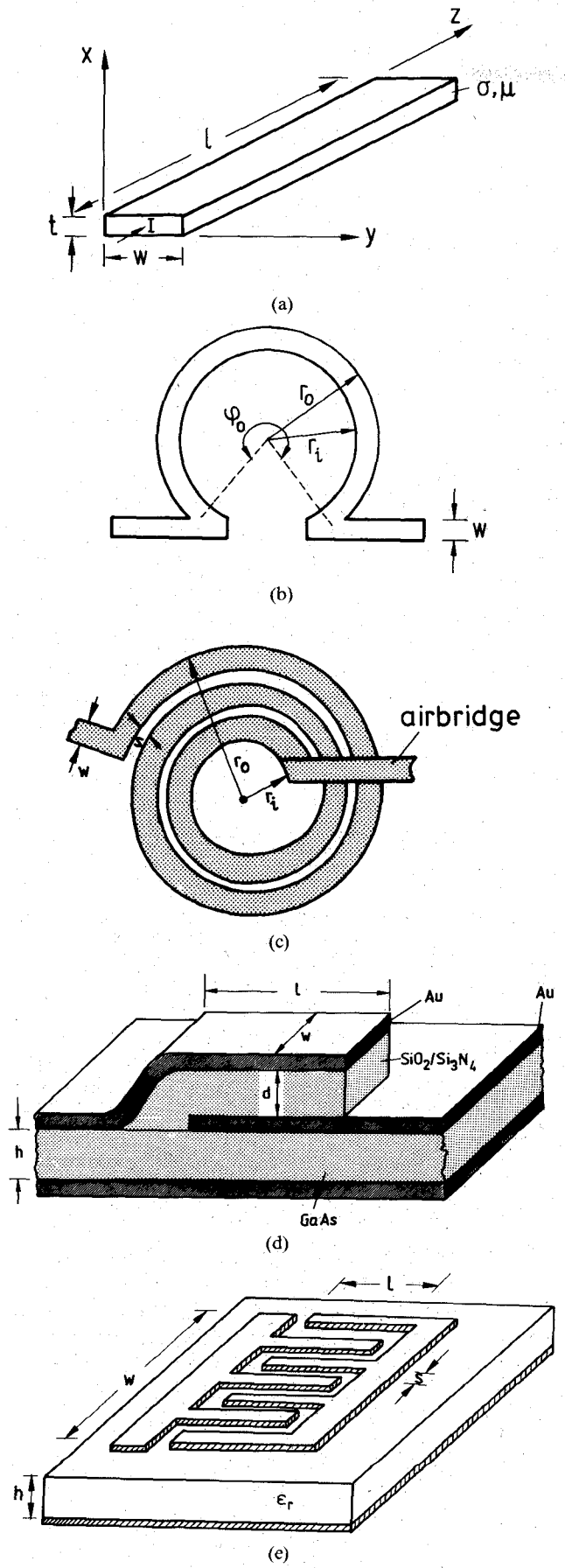

Fig. 1. Schematic representation of (a) a straight line, (b) a single loop inductor, (c) a circular spiral inductor, (d) an interdigitated capacitor, and (e) a MIM-capacitor.

TABLE I
FREQUENCY-DEPENDENT RESISTANCE R_{ac} OF A METALLIC STRIP WITH RECTANGULAR CROSS SECTION (WIDTH w, THICKNESS t) NORMALIZED TO THE dc RESISTANCE R_{dc} AS A FUNCTION OF THE NORMALIZED FREQUENCY $x_w = (2f\sigma\mu wt)^{1/2}$

x_w \ w/t	1	2	4	6	12	18
0.5	1.000	1.000	1.000	1.001	1.001	1.000
1.0	1.006	1.007	1.007	1.008	1.008	1.005
1.5	1.030	1.032	1.035	1.038	1.039	1.025
2.0	1.090	1.093	1.096	1.100	1.098	1.062
2.5	1.201	1.198	1.187	1.186	1.173	1.110
3.0	1.361	1.339	1.294	1.284	1.253	1.161
3.5	1.554	1.503	1.411	1.386	1.333	1.213
4.0	1.757	1.680	1.539	1.495	1.414	1.264
4.5	1.957	1.866	1.678	1.613	1.496	1.317
5.0	2.152	2.057	1.829	1.745	1.581	1.370
5.5	2.342	2.250	1.990	1.876	1.669	1.425
6.0	2.531	2.441	2.160	2.008	1.763	1.482
6.5	2.720	2.631	2.335	2.159	1.861	1.541
7.0	2.910	2.818	2.514	2.316	1.965	1.604
7.5	3.101	3.005	2.694	2.480	2.077	1.671
8.0	3.292	3.192	2.873	2.646	2.194	1.742
8.5	3.484	3.379	3.052	2.815	2.318	1.818
9.0	3.676	3.568	3.228	2.984	2.448	1.898
9.5	3.868	3.757	3.404	3.153	2.583	1.983
10.0	4.061	3.948	3.580	3.320	2.718	2.073
10.5	4.254	4.140	3.755	3.486	2.853	2.167
11.0	4.446	4.333	3.930	3.650	2.989	2.266
11.5	4.639	4.527	4.107	3.812	3.124	2.369
12.0	4.833	4.722	4.284	3.973	3.259	2.476

width w may be of the order of the metallization thickness t and additionally that the metallization thickness (especially at lower frequencies) is no longer large compared to the skin depth. The approximate loss calculations as they have been used in MIC's [15] therefore normally result in calculated Q factors which are too high compared to measurements. The exact calculation of the frequency-dependent resistance of a metallic conductor with rectangular cross section is a very difficult task and can be done only using sophisticated numerical methods [14]. Therefore for the application in CAD programs, measurements which have been published by Haefner [13] are fitted by the following closed formula:

$$R = \frac{l}{\sigma wt}\left\{\frac{0.43093x_w}{1+0.041(w/t)^{1.19}} + \frac{1.1147+1.2868x_w}{1.2296+1.287x_w^3} + 0.0035(w/t-1)^{1.8}\right\} \quad \text{(1a)}$$

for $x_w \geqslant 2.5$ and

$$R = \frac{l}{\sigma wt}\left\{1+0.0122x_w^{(3+0.01x_w^2)}\right\} \quad \text{(1b)}$$

for $x_w < 2.5$ and with $x_w = (2f\sigma\mu wt)^{1/2}$ a normalized frequency. The formulas describe the conductor resistance with an accuracy between 3 percent and 5 percent in the range $w/t < 12$ and $x_w < 20$. In the range $2.0 \leqslant x_w \leqslant 3.0$, the results of (1a) and (1b) additionally are fitted by approximating, smoothing curves. In (1) l is the length, w the line width, and t the metallization thickness of the conductor. Moreover σ and μ stand for the conductivity and the permeability of the conductor material. If a two-layer metallization with a thin adhesive layer ($t < 0.5$ μm) is used, (1) also can be used to calculate the resultant resistance of this structure by parallel shunting the two resultant resistances of the layers.

If a higher accuracy than that given by (1) is needed for loss calculations, look-up tables can be generated from the numerical methods which have been developed [14]. Table I shows such numerical results for the resistance of a

conductor of rectangular cross section. It shows that the skin effect essentially influences the resistance in a complicated way which cannot be described with the methods used up to now [15].

B. The Straight-Line Inductor

The static self-inductances and mutual inductances of a conductor system carrying the current densities $\vec{S}_m$ and $\vec{S}_n$ over their cross sections A_m and A_n are given by [16]

$$L_{mn} = \frac{\mu}{4\pi i_m i_n} \iint_{A_m} \iint_{A_n} \oint_{C_m} \oint_{C_n} \frac{\vec{S}_m \cdot \vec{S}_n}{r_{mn}} ds_n ds_m dA_n dA_m. \quad (2)$$

Principally this integral must be solved to find an exact solution for the inductances. In the case of a flat straight conductor of line width w, length l, and zero metallization thickness t, an exact evaluation of (2) can be found [17], [18] by

$$L = \frac{\mu_0 l}{2\pi}\left\{\operatorname{arsinh}\left(\frac{l}{w}\right) + \frac{l}{w}\operatorname{arsinh}\left(\frac{w}{l}\right) + \frac{w}{3l} - \frac{1}{3}\left(\frac{l}{w}\right)^2\left[\left(1+\frac{w^2}{l^2}\right)^{3/2} - 1\right]\right\} \quad (3)$$

which also considers the mutual inductance between different parts of the conductor. Caulton *et al.* [1] have shown that the influence of the metallization thickness t can be considered approximately in calculating static inductances of flat conductors if the line width w is replaced by $w + t$. If this is done in (3), the following formula results:

$$L = \frac{\mu_0 l}{2\pi}\left\{\operatorname{arsinh}\left(\frac{l}{w+t}\right) + \frac{l}{w+t}\operatorname{arsinh}\left(\frac{w+t}{l}\right) + \frac{w+t}{3l} - \frac{1}{3}\left(\frac{l}{w+t}\right)^2\left[\left(1+\frac{(w+t)^2}{l^2}\right)^{3/2} - 1\right]\right\} \quad (4)$$

which approximates the static inductance of a flat conductor quite accurately as long as the line width w is much larger than the metallization thickness t.

In lumped elements the line width and the metallization thickness often are of the same order. In this case (4) cannot be used. Ollendorff [19] described a solution of the inductance integral applying the method of medium geometrical distances, which can be used to calculate the static inductance of a conductor with arbitrary rectangular or quadratic cross section:

$$L = \frac{\mu_0 l}{2\pi}\left[\ln\left(\frac{2l}{\rho}\right) - 1\right] \quad (5)$$

with

$$\ln\left(\frac{\rho}{c}\right) = \frac{1}{A^2}\iint_{A_1}\iint_{A_2} \ln\frac{x}{c}\, dA_1\, dA_2. \quad (6)$$

Equation (6) describes the medium value of the geometrical distance between two arbitrary points of distance x in the areas dA_1 and dA_2 in the cross section A of the conductor. The solution of (6) in the case of a rectangular conductor is given by

$$\ln\left(\frac{\rho}{2c}\right) = -\frac{25}{12} - \frac{1}{6}\left\{\left(\frac{w}{t}\right)^2 \ln\sqrt{1+\left(\frac{t}{w}\right)^2} + \left(\frac{t}{w}\right)^2 \ln\sqrt{1+\left(\frac{w}{t}\right)^2}\right\} + \frac{2}{3}\left\{\frac{w}{t}\arctan\left(\frac{t}{w}\right) + \frac{t}{w}\arctan\left(\frac{w}{t}\right)\right\} \quad (7)$$

with $2c = (w^2 + t^2)^{1/2}$.

The formulas given above do not consider the inhomogeneous and frequency-dependent current density over the cross section of the conductor as it is predicted by skin effect theory. The outer inductance of the conductor is for the most part not influenced by this changing current density. The inner inductance normally is very small compared to the outer inductance, so that its influence on the total inductance is negligibly small. If it is to be considered, it can be found approximately from a skin effect theory by calculating the complex power transported through the cross section of the conductor and identifying the imaginary part of this power with $0.5\omega L_i I^2$, where I is the total current through the cross section. In this way an approximate solution for L_i and for $w > t$ can be found as

$$L_i = \frac{\mu_0 l}{4mw}\frac{\sinh(mt) - \sin(mt)}{\cosh(mt) - \cos(mt)} \quad (8)$$

with $m = (\pi f \sigma \mu)^{1/2}$. In the case of a conductor with quadratic cross section, the formula

$$L_i = \frac{lm^2}{8\sigma\omega}\frac{\sinh^2(m'w) - \sin^2(m'w)}{[\cosh(m'w) - \cos(m'w)]^2}, \qquad m' = m/\sqrt{2} \quad (9)$$

can be used.

The frequency-dependent total inductance of the straight line is found as the sum of the frequency-independent outer inductance and the frequency-dependent inner inductance.

C. The Single-Loop Inductor

The single-loop inductor of inner radius r_i and outer radius r_o and with a length described by the angle φ_0 (Fig. 1(b)) already is a very complicated structure if the mutual inductances between the different loop segments are to be considered exactly. For the case of the inductor with zero metallization thickness, the inductance integral (2) can be reduced to the fourfold integral

$$L = \frac{\mu_0}{4\pi w^2}\int_{r_i}^{r_o}\int_{r_i}^{r_o}\int_0^{\varphi_0}\int_0^{\varphi_0} H\, dr_1\, dr_2\, d\varphi_1\, d\varphi_2 \quad (10a)$$

with

$$H = \frac{r_1 r_2 \cos(\varphi_2 - \varphi_1)}{\sqrt{r_1^2 + r_2^2 - 2r_1 r_2 \cos(\varphi_1 - \varphi_2)}}. \quad (10b)$$

As has been shown by Hentschel [17], [18], this integral can be reduced to a onefold integral which (avoiding an error in the work of Hentschel) can be written in the form

$$L = \frac{\mu_0}{2\pi w^2}\int_0^{\varphi_0/\sqrt{2}} \left(\varphi_0\sqrt{2} - 2\varphi\right)\cos\left(\sqrt{2}\,\varphi\right)F(\varphi)\,d\varphi \quad (10c)$$

and which can be solved numerically. In (10c), $F(\varphi)$ has the meaning

$$F(\varphi) = G(r_1, r_2)\big|_{r_1=r_i}^{r_o}\big|_{r_2=r_i}^{r_o} \quad (10d)$$

with

$$G(r_1, r_2) = \frac{1}{3}R^3 + \frac{2}{3}r_1 r_2 R\cos\left(\sqrt{2}\,\varphi\right) + \frac{2}{3}r_1^3\cos\left(\sqrt{2}\,\varphi\right) \cdot \operatorname{arsinh}\frac{r_2 - r_1\cos\left(\sqrt{2}\,\varphi\right)}{r_1\left|\sin\left(\sqrt{2}\,\varphi\right)\right|}$$

$$R = \sqrt{r_1^2 + r_2^2 - 2r_1 r_2\cos\left(\sqrt{2}\,\varphi\right)}$$

$$G(r_1, r_2)\big|_{r_1=r_i}^{r_o}\big|_{r_2=r_i}^{r_o} = G(r_o, r_o) - G(r_i, r_o) - G(r_o, r_i) + G(r_i, r_i). \quad (10e)$$

The metallization thickness t again can be considered approximately in (10c) if an effective width $w + t$ is used. In the case where the single-loop inductor has a ground metallization on the backside of the substrate material, the capacitive effects on the ground metallization lead to a remarkable frequency dependence in the inductor parameters. This frequency dependence is modeled in the same way as that described for the circular and rectangular spiral inductor in the next section.

D. Circular and Rectangular Spiral Inductors

The circular and rectangular spiral inductors have been modeled using the principle which will be described below. For calculating the static inductance of these planar coils, a similar method has been used by Remke and Burdick [20] in the case of the circular spiral inductor. Fig. 2 shows the basical considerations in the example of the rectangular spiral inductor: The total spiral inductor is broken into n line segments, which are straight lines in the case of the rectangular spiral inductor and circular one-turn elements as described in Section II-C in the case of the circular spiral inductor. The static inductances $L_i (i = 1, 2, \cdots, n)$ of these segments are calculated using the methods described above. The mutual inductances M_{ij} between two different line segments in the case of the straight line segments can be found exactly if the metallization thickness is assumed to be zero; in the case of the circular line segments the inductances can be approximated by known evaluations of the inductance integral if the line segments are considered as line currents. In the case of the rectangular spiral inductor, the mutual inductance can be positive or negative depending on the current direction in the different line sections. For the mutual inductances between the ith and

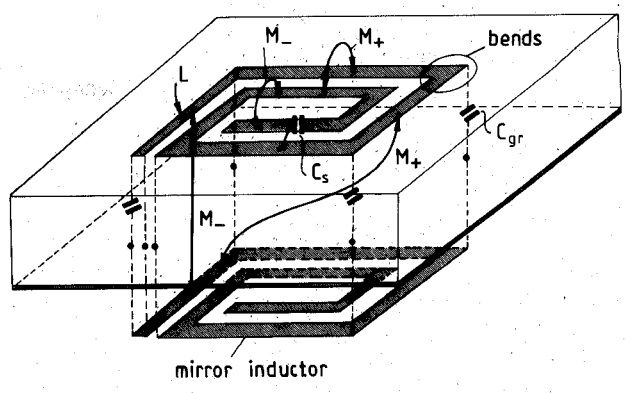

Fig. 2. Inductances and capacitances of the rectangular spiral inductor on a substrate with metallized ground plane, considered in the computer model.

jth circular line segment in the case of the circular spiral inductor, the evaluation of Neumann's formula

$$M = \frac{\mu}{4\pi}\oint_C\oint_{C'}\frac{d\vec{l}_1\,d\vec{l}_2}{r} \quad (11a)$$

which already has been used in [20], is applied:

$$M_{ij} = \mu\sqrt{ab}\left[\left(\frac{2}{k_{ij}} - k_{ij}\right)K(k_{ij}) - \frac{2}{k_{ij}}E(k_{ij})\right] \quad (11b)$$

with $k_{ij} = 4ab/(a+b)^2$, $a = r_i + (i - 0.5)(w + s)$, $b = r_i(j - 0.5)(w + s)$, r_i the inner radius of the circular spiral inductor, and s the gap width between the turns. In the case of two coupled straight thin film strips of width w, length l, and zero metallization thickness, the mutual inductance is given by [17], [18]

$$M = \frac{\mu l}{4\pi}\left(\frac{l}{w}\right)^2\left[F(q)\big|_{q=(w+s)/l}^{q=s/l} + F(q)\big|_{q=(w+s)/l}^{q=(2w+s)/l}\right] \quad (12a)$$

with

$$F(q) = q^2\operatorname{arsinh}\left(\frac{1}{q}\right) + q\operatorname{arsinh}(q) + \frac{q^3}{3} - \frac{1}{3}\left(1 + q^2\right)^{3/2}. \quad (12b)$$

If additionally the substrate material is metallized on its ground plane, the mutual inductances M_{ij}^m between the original coil and a mirror coil under the ground plane must be taken into account. For the circular spiral inductor they are of the form

$$M_{ij}^m = \mu\sqrt{ab}\left[\left(\frac{2}{k_{ij}} - k_{ij}\right)K(k_{ij}) - \frac{2}{k_{ij}}E(k_{ij})\right] \quad (13a)$$

with $k_{ij} = 4ab/(4h^2 + (a+b)^2)$ and the values for a and b given above. In (11b) and (13a), $K(k)$ and $E(k)$ are the complete elliptical integrals of the first and second kind:

$$K(k) = \int_0^{\pi/2}\frac{d\varphi}{\left(1 - k^2\sin^2\varphi\right)^{1/2}}$$

$$E(k) = \int_0^{\pi/2}\left(1 - k^2\sin^2\varphi\right)^{1/2}d\varphi. \quad (13b)$$

The total static inductance of the spiral inductor then is

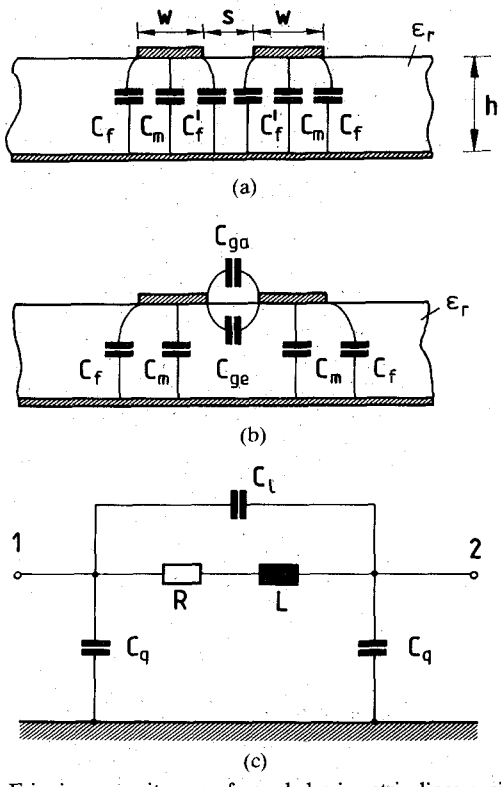

Fig. 3. Fringing capacitances of coupled microstrip lines excited in (a) the even mode and (b) the odd mode, used for the modeling of the capacitive effects in spiral inductors. (c) Equivalent circuit of a line segment and the spiral inductors.

found in a way similar to that described in [20]:

$$L = \sum_{i=1}^{n} L_i + 2 \sum_{i=1}^{n-1} \sum_{j=i+1}^{n} M_{ij} + \sum_{i=1}^{n} \sum_{j=1}^{n} M_{ij}^{m}. \quad (14)$$

To model the frequency behavior of the spiral inductors correctly, the capacitive effects between the line segments and from the line segments to the ground plane must be taken into account. The fringing capacitances (Fig. 3) between the lines and to the ground plane can be found from classical microstrip theory. For example the capacitances C_f, C_m, C_f' of coupled microstrip lines excited in the even mode and the capacitances C_f, C_m, C_{ge}, and C_{ga} of coupled microstrip lines excited in the odd mode have been approximated by simple formulas, e.g. by Garg and Bahl [25]:

$$C_{ga} = \frac{\epsilon_0}{2} \frac{K(k')}{K(k)} \quad (15a)$$

where $K(k)$ again is the complete elliptical integral, $K(k')$ is its complement, $k = s/h(s/h + 2w/h)$, and $k' = (1 - k^2)^{1/2}$:

$$C_{ge} = \frac{\epsilon_0 \epsilon_r}{\pi} \ln \left[\coth \left(\frac{\pi}{4} \frac{s}{h} \right) + 0.65 C_f \left[\frac{0.02}{s/h} \epsilon_r^{1/2} + 1 - \epsilon_r^{-2} \right] \right]. \quad (15b)$$

C_m is the main capacitance of a microstrip line of width w on a substrate of height h and with the relative dielectric constant ϵ_r:

$$C_m = \frac{\epsilon_0 \epsilon_r w}{h} \quad (15c)$$

and the fringing capacitance C_f' can be found from

$$C_f' = \frac{C_f}{1 + A(h/s) \tanh(8s/h)} \quad (15d)$$

with $A = \exp\{-0.1 \exp(2.33 - 2.53w/h)\}$ and $C_f = 0.5\{\epsilon_{\text{eff}}^{1/2}/(c_0 Z_0) - \epsilon_0 \epsilon_r w/h\}$. Here c_0 is the velocity of light in free space, Z_0 is the frequency-dependent characteristic impedance of a microstrip line of width w on a substrate described above, and ϵ_{eff} is the frequency-dependent effective dielectric constant of this line (e.g. [26]).

The different inductive and capacitive elements of each line segment are combined in a suitable manner so that the physical behavior of the spiral inductor is modeled approximately. It must however be mentioned that a certain arbitrariness cannot be avoided in this modeling technique, because, for example, the mutual inductances cannot be connected to just one line element, but they are a property of the total, distributed coil. From these considerations, an equivalent circuit of the form shown in Fig. 3(c) can be found for each line segment in the case of the rectangular spiral inductor or for each turn in the case of the circular spiral inductor. The air bridge which normally is used for connecting the inner inductor node to the circuit can additionally be considered by its inductance and capacitive effects between the air bridge and the inductor segments. The total equivalent circuit of the spiral inductor, which is of the same form as shown in Fig. 3(c), can be found by classical circuit theory.

In addition to the modeling described above, the inductance of the rectangular spiral inductor also has been modeled by a line theory as it for the first time has been described by Camp *et al.* [27] and Cahana [28]. Their models have been improved [29] and compared to the results of the simpler theory given above. Good agreement is found between both modeling techniques.

E. The MIM Capacitor

The capacitance of the MIM (metal–insulator–metal) capacitor easily and most accurately can be described by the capacitance of a rectangular plate capacitor if the thickness of the insulating material is very small (e.g., 0.1 μm to 1 μm). For thicker insulating materials the influence of the stray field can be taken into account by using Chang's [36] conformal mapping technique.

To analyze the frequency dependence of the MIM capacitance, the capacitor was considered to be an open microstrip line, and with convenient theories [37] the input impedance and thus the capacitance of the structure were determined. As a result the frequency dependence is negligible and should only be considered in those cases where the dielectric layer is unusually thick and the length of the electrode is larger than one tenth of a wavelength.

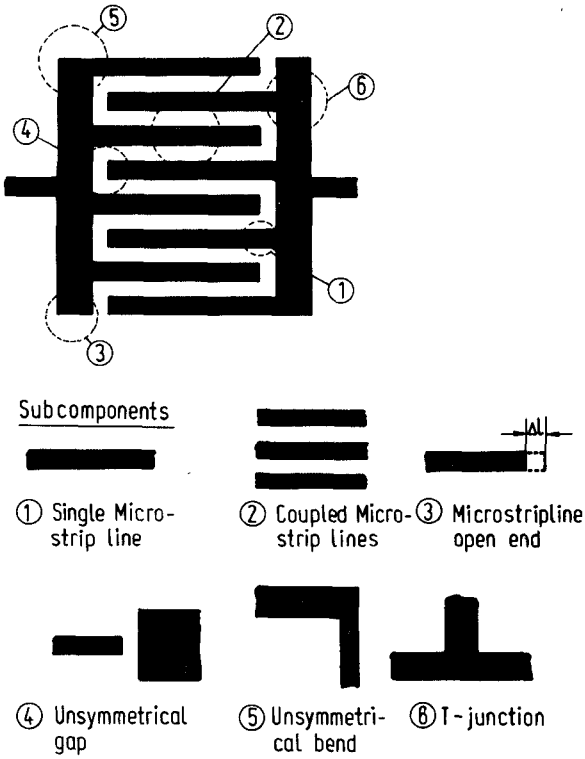

Fig. 4. The interdigitated capacitor and its subcomponents.

F. The Interdigitated Capacitor

In 1970, Alley [38] published the first advanced model for the interdigitated capacitor. His model is based on a lossless coupled microstrip line theory. It is in this respect an approximate model, as it calculates the total admittance of the parallel shunted fingers of the capacitor without considering the different positions of these fingers. The admittance then is considered to be uniformly parallel shunted to the main line of the capacitor. The model does not consider the phase shift along the main line, which may be large if a capacitor with high finger number is used, and it does not take into account the influence of the discontinuities incorporated into the structure, e.g., the open ends of the lines, the gaps, and the T-junctions.

In 1979, Hobdell [39] introduced a loss calculation into Alley's theory, and in 1983 Esfandiari *et al.* [40] gave additional information about the influence of the metallization thickness on the capacitance and the Q factor.

In this paper an improved model which is based on [29] is used. The interdigitated capacitor is divided into its basic subcomponents, as is shown in Fig. 4: the single microstrip line, coupled microstrip lines, the microstrip open end, the microstrip unsymmetrical gap, the unsymmetrical microstrip 90° bend, and the microstrip T-junction. Computer models for all these elements are available and are used to compose the interdigitated capacitor using known methods of S-parameter network theory [33]. Using this new model, the mentioned restrictions of Alley's model can be overcome and the model is applicable even at high frequencies because all dispersive effects have been taken into account.

III. Experimental Results

A. Measurement Procedures and Test Structures

The measurement process used includes the S-parameter characterization up to 12 GHz and the resonator frequency shift (RFS) method applied up to 18 GHz. The RFS method [42] is a differential measurement with, on the one hand, a well-known microstrip reference resonator and, on the other hand, a resonator that is perturbed after the specimen to be tested is inserted. The advantage of this method is the accurate and separate determination of series and shunt equivalent circuit elements (Fig. 5) by considering the even- and odd-numbered resonances. The RFS method was indispensable for the measurement of low inductance and capacitance values.

Fig. 6(a) shows the computer-controlled measurement setup with the PC, the sweeper, the frequency counter, and the power meter. The equivalent circuits of the test setup for the two cases (series/shunt) are illustrated in Fig. 6(b)–(d). The most important interfaces—coupling gap and bond wires—are individually examined and considered with a computer correction program. The fabrication tolerances of the resonators are usually negligible compared to the dominant influence of bond wire tolerances. Assuming a tolerance of ± 10 percent in bond wire length measurement ($L' = 0.65$ nH/mm; $l/2 \approx 0.3$ mm, $\varnothing = 17.5$ μm), the characterization of straight line inductors with $L \approx 0.1$ nH already shows an inaccuracy of 40 percent. The investigation of a very small interdigitated capacitor ($C = 0.1$ pF) in the shunt connection gives for comparison only an inaccuracy of 5 percent between model and experiment assuming the same bond wire tolerance. Two mask sets were designed with respect to intensive scaling investigations. They contain the following structures: (1) MIM capacitors, realized with Si_3N_4 dielectric and air bridge interconnection, and covering a value range of about 0.1–30 pF via different dielectric layer thickness ($t = 180$–500 nm). (2) Interdigitated capacitors, which are fabricated on GaAs with TiAu plating base and 5 μm plated gold. The planned value range was 0.01 to 0.5 pF, the structures contained different finger length, width, gap, and number. (3) Straight line, single-loop and spiral inductors fabricated similar to the interdigitated capacitors but with an additional air bridge as interconnection to the bond pad in the case of the spiral inductors. The covered value range was about 0.01 to 8 nH. (4) Moreover some resonant circuits for the derivation of Q-factors were included.

B. Experimental Verification

1) Spiral Inductor (Circular Shape): Two different structures with 3.5 and 2.5 turns were experimentally examined over a broad frequency range. As a result of previous investigations and compromise between chip size and a sufficient high quality factor, a geometry with an inner diameter of 115 μm, a conductor width of 20 μm, and a conductor space of 15 μm was selected. Fig. 7 shows the frequency behavior of the largest inductor with 3.5 turns.

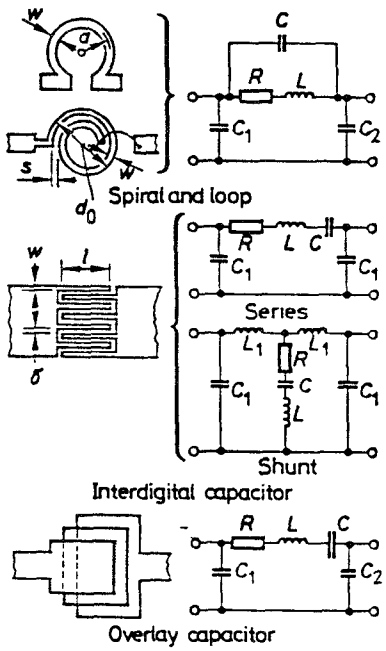

Fig. 5. Equivalent circuits of lumped elements.

It contains the S-parameter results of three elements, two curves derived by RFS measurement, and the model calculation. The resonant frequency of this inductor is about 12 GHz, the recommended usable frequency range is $\leqslant 8$ GHz, and the deviation between model and measurement is $< \pm 5$ percent in this range. The experimental and theoretical results of the second structure ($n = 2.5$ turns) show a resonant frequency of 18 GHz, a useful frequency range of about 14 GHz, and a deviation from model $< \pm 6$ percent (Fig. 7). Table II shows the equivalent circuit elements (Fig. 5) of the spiral inductors.

2) Single-Loop Inductor: Two different structures with an inner radius of 75 μm and a loop of either 360° or 216° were examined in a frequency range of about 1 to 18 GHz. In one case 12 and in the other case seven resonant frequencies were investigated using resonators of different lengths. The measurement results together with the theoretical curves derived by the new model are illustrated in Fig. 8. Both structures are useful in the complete frequency range. The frequency dependence is relatively weak, a rise of 15 percent for the larger element being visible and about 7 percent for the smaller inductor. The deviation between model and experiment is $\leqslant 15$ percent.

3) Interdigital Capacitors: The analyzed structures show a finger length of 100 μm, a finger width of 10 μm, and a finger gap of 10 (5) μm, the number of fingers being $n = 50$, 20, 10, and 5. The frequency-dependent capacitances are visible in Figs. 9–11. These illustrations contain the capacitor values derived by two models together with the measured curves using the S-parameter and RFS method. The resonant frequency of the largest capacitor is about 18 GHz (model of Wolff) and 14 GHz (model of Esfandiari), respectively. For this structure the deviation between both models and experiment is $< \pm 5$ percent below 8 GHz and about ± 10 percent up to 12 GHz (Fig. 9). The same deviation, $\leqslant \pm 5$ percent up to 12 GHz, is

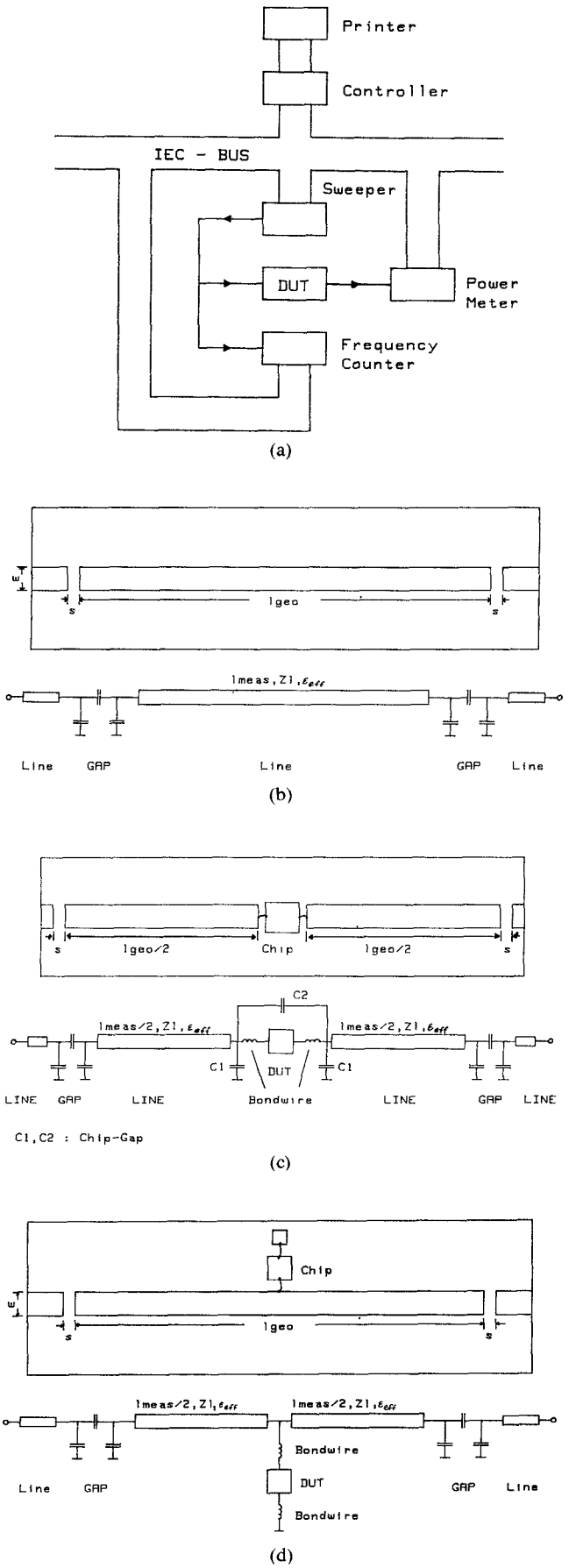

Fig. 6. Measurement setup (a) and equivalent circuit of the resonator frequency shift method; (b) reference resonator; (c) series resonator with DUT; (d) shunt resonator with DUT.

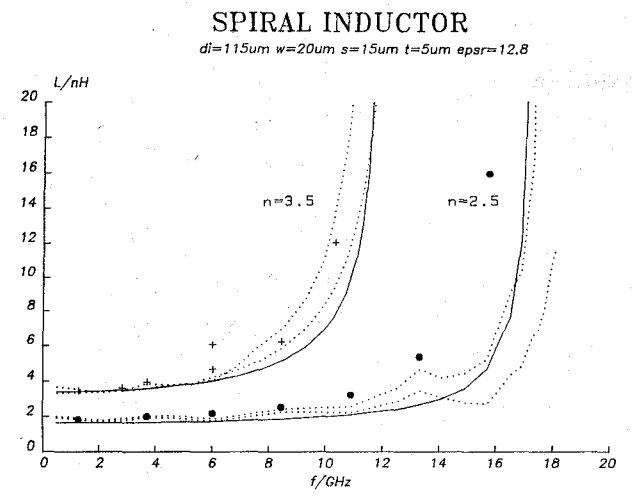

Fig. 7. Frequency behavior of a circular spiral inductor ($n = 2.5, 3.5$). Comparison between model and experiment. —— theory; +/● RFS measurement; --- *S*-parameter measurement.

TABLE II
VALUES OF THE EQUIVALENT CIRCUIT ELEMENTS OF SPIRAL INDUCTORS

n	w/um	s/um	ri/um	L/nH	R/Ω	C1/fF	C2/fF	C/fF
1.5	20	15	57.5	0.61	0.75	20	30	48
2.5	20	15	57.5	1.70	1.70	45	62	50
3.5	20	15	57.5	3.40	2.20	70	100	55
4.1	15	15	60.0	4.40	3.70	70	115	74

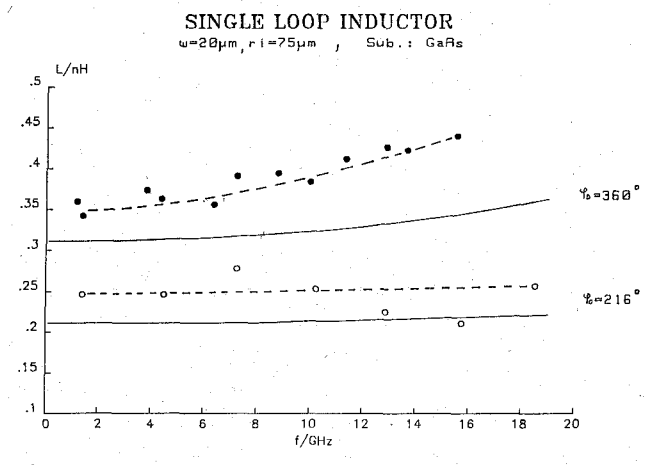

Fig. 8. Frequency dependence of a single-loop inductor ($\varphi_0 = 216°, 360°$). Comparison between model and experiment. —— theory; -○- -●- RFS measurement, ri = 75 μm, w = 20 μm, t (metal) = 5 μm, h (substrate) = 150 μm.

given for the second element ($n = 20$, Fig. 10). In this case a miniaturization down to a gap of only 5 μm is also considered, and the illustration reveals an increased inaccuracy of the Esfandiari model. Fig. 11 finally shows that even very small capacitors with only 10 fingers and a value of 0.08 pF can be modeled with an accuracy of 90 to 95 percent up to about 16 GHz. Only in the case of the smallest element ($n = 5, C \approx 0.04$ pF) are all measured values about 25 percent above the calculated results. It should be mentioned that the approximation formula of Joshi [9] shows already at low frequencies a mistake of 30–40 percent depending on the structure size. Table III shows the equivalent circuit elements (Fig. 5) of the interdigital capacitors.

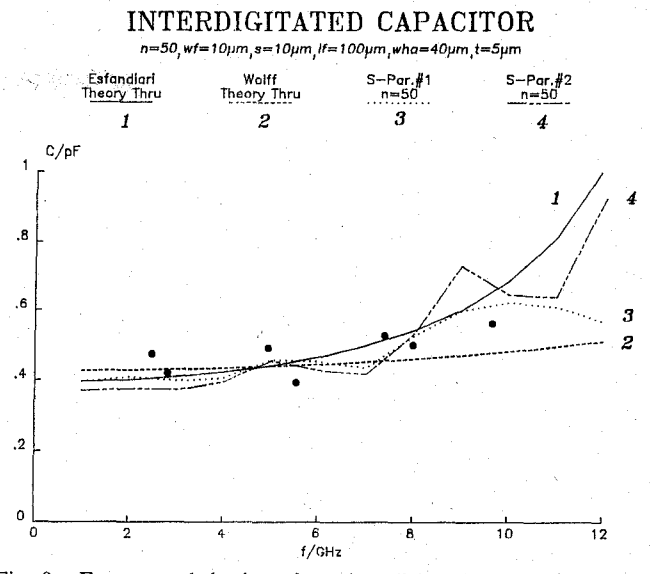

Fig. 9. Frequency behavior of an interdigitated capacitor ($n = 50$). Comparison between model and experiment.

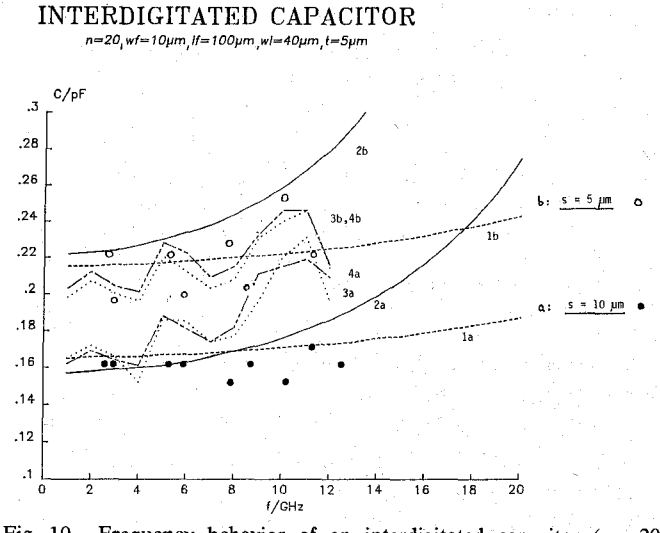

Fig. 10. Frequency behavior of an interdigitated capacitor ($n = 20$, $s = 5$ or 10 μm). Comparison between model and experiment. Model of Esfandiari (2), model of this work (1), *s*-parameter measurement (3,4), RFS measurement (○,●).

4) MIM Capacitors: Exact measurements with the impedance analyzer at $\leqslant 13$ MHz and *S*-parameter analysis up to 1 GHz show in good accordance a deviation between model and experiment of $\leqslant \pm 6$ percent. The examined structures had capacitor values between 0.4 and 10 pF. The frequency dependence up to 12 GHz was measured with the RFS method, but did not deliver useful results. Parasitic elements, especially the wire inductance, dominate the evaluation.

5) Straight-Line Inductor: The experimental verification was done with three different structures of 40 μm width and lengths of $l = 110$ μm ($L_{\text{theor}} = 0.053$ nH), $l = 270$ μm ($L_{\text{theor}} = 0.16$ nH), and $l = 790$ μm ($L_{\text{theor}} = 0.6$ nH) in a frequency range of about 2 to 18 GHz. Unfortunately, the test ceramic of the largest element was only a provisional structure, which results in incorrect high-frequency performance.

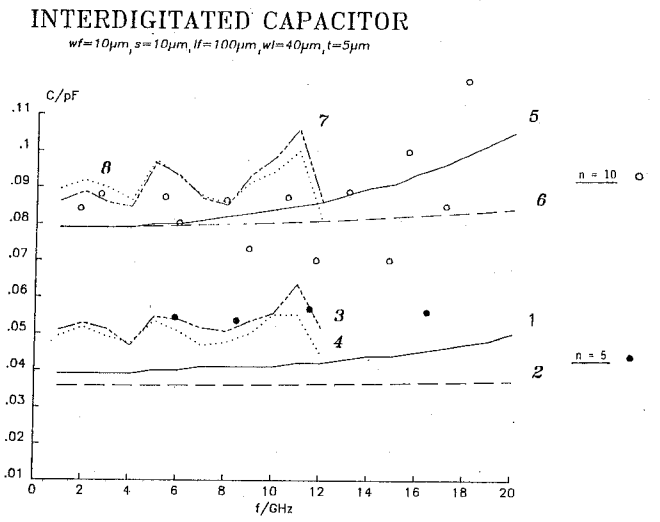

Fig. 11. Frequency behavior of an interdigitated capacitor ($n=10,5$). Comparison between model and experiment. Model of Esfandiari (1,5), model of this work (2,6), s-parameter measurement (3,4,7,8), RFS measurement (○,●).

TABLE III
VALUES OF THE EQUIVALENT CIRCUIT ELEMENTS OF INTERDIGITAL CAPACITORS

f/GHz	0		3		6		9		12		15		18	
n	C	Cl	C	Cl	C	Cl	C	Cl	C	Cl	C	Cl	C	Cl
5	.036	.018	.036	.018	.036	.018	.036	.018	.036	.018	.037	.019	.037	.019
10	.079	.021	.079	.021	.080	.021	.080	.022	.081	.022	.082	.022	.083	.022
20	.165	.027	.166	.027	.167	.027	.170	.028	.173	.028	.177	.028	.183	.029
50	.425	.044	.430	.044	.444	.045	.469	.046	.509	.047	.575	.048	.685	.048
205	.215	.012	.216	.012	.218	.014	.221	.017	.225	.019	.230	.022	.237	.024

While the experimental results with the smallest element did not show the necessary accuracy, the larger inductor measurement revealed useful values. With the above-mentioned restrictions the model results are roughly 20 to 30 percent above the experimental. This is reasonable with respect to the fact that about half of the mistake is already a result of the uncertainty of the bond wire inductance.

6) Q Factors: The calculated Q factors based on dc measured ohmic losses of the analyzed spiral inductors are illustrated in Fig. 12 versus frequency. In the case of the smallest structure ($n=1.5$), we plotted additional values derived by the evaluation of resonant circuits. The important information is that the measured Q factors are a factor of 0.6 ± 0.1 below the calculated, which results in approximately $Q=15$ at 2 GHz and $Q_{max}=35$ at higher frequencies. This situation is mainly a result of unwanted ohmic losses. A similar procedure for the single-loop inductor is also visible in Fig. 12. Again the Q factors are of the same value, but with improved high-frequency behavior. The results including dominant ohmic losses are confirmed by Pengelly [12].

Finally, the frequency-dependent calculated Q factors of interdigital and MIM capacitors are illustrated in Fig. 13. From the resonant circuit measurements we derived a Q factor of about 50 for the interdigitated capacitor with 20 fingers. This corresponds to the theoretical values assuming a loss tangent of 0.01 for the semi-insulating GaAs and

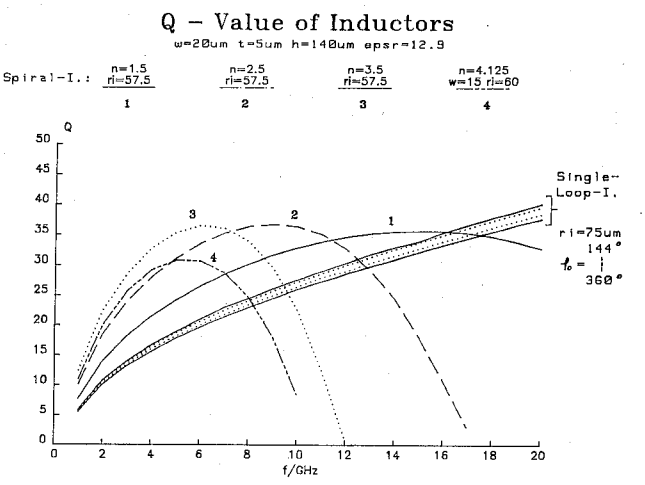

Fig. 12. Single- and spiral loop inductor. Calculated Q factors based on measured ohmic losses and results of resonant circuit measurements (○).

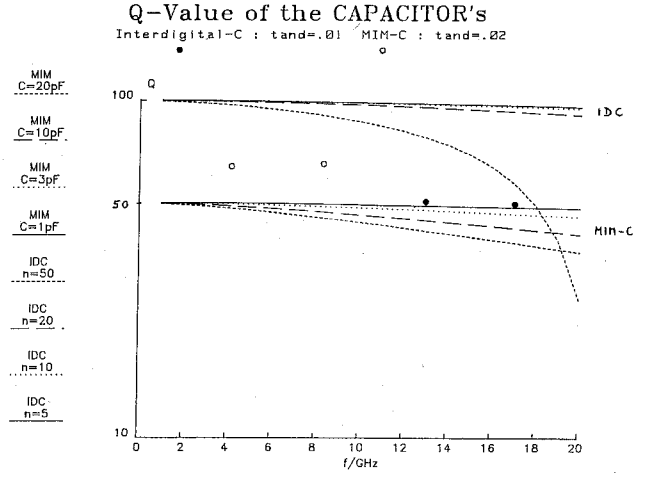

Fig. 13. Interdigitated and MIM capacitors. Calculated Q factors and results of resonant circuit measurements (○,●).

SiN dielectric. The measured results are similar to those published by Pengelly [12] and are of the same order of magnitude as those reported by Esfandiari *et al.* [40]. In this case not only ohmic but also substrate losses must play an important role. The measured Q factors of two MIM capacitors ($C=0.4$ pF and $C=1.4$ pF) as part of a resonant circuit were about 65 ± 15, which is in accordance with the model assuming a loss tangent of 0.02 for the dominant dielectric.

IV. CONCLUSIONS AND SUMMARY

Advanced models for lumped-element inductors and capacitors were derived by the application of state-of-the-art stripline theory and network analysis. In addition, the basic inductor elements were simulated by the numerical solution of the inductance integral. Thus, equivalent circuits for the lumped elements containing all main values and parasitics are available (Fig. 5).

A broad experimental verification of all models up to 18 GHz with extensive scaling investigations and improved test procedures was applied. The basic data for integrable

TABLE IV
RESULTS OF PASSIVE LUMPED ELEMENTS ($f = 1$–18 GHz)

Element	Useful MMIC values	Q 2 GHz	Q 12 GHz	Q 18 GHz	Dev. Exp / CAD %
Spiral Inductor	L = 1 - 5 nH	12	30	-	< ± 5
Single-Loop Inductor	L = 0.2 - 0.5 nH	12	30	35	< ± 10
Straight Line Inductor	L = 0.05 - 0.2 nH	18	40	50	< + 10
Interdigital Capacitor	C = 0.1 - 0.6 pF		50	50	≤ ± 5
	C = 0.02 - 0.05pF				< + 10
MIM-Capacitor	C = 0.5 - 20 pF	65	65	?	≤ ± 5

passive microwave elements are listed in Table IV, showing first and foremost a restricted range of values against the data frequently published, a high model accuracy even for very small elements, and a useful frequency range beyond *X*-band for lumped elements besides multiturn inductors. For some applications the relatively low Q factors (about 100) of lumped elements in a convenient MMIC layout may be unacceptable. A further important aspect at the beginning of MMIC design is deciding between lumped and distributed elements in those cases where the value range overlaps. Such studies, which centralize in our case mainly to topology questions, are in progress. A comparison between circular and rectangular spiral inductors to study especially bend effects is also under investigation. Passive MMIC's—couplers, filters, matching networks—based on the as-derived lumped-element and involved distributed-element models have been realized in the frequency range 1–18 GHz. The results of IF filters for the frequency range 0.95–1.75 GHz and broad-band 12 GHz and 18 GHz Lange coupler verify the high model accuracy and useful layout. The measured insertion loss was 1.5 dB for the filter and 0.65 dB (1.5 dB) additional insertion loss in the coupling path of the 12 GHz (18 GHz) coupler.

REFERENCES

[1] M. Caulton, S. P. Knight, and D. A. Daly, "Hybrid integrated lumped-element microwave amplifiers," *IEEE Trans. Electron Devices*, vol. ED-15, pp. 459–466, 1968.

[2] F. E. Terman, *Radio Engineer's Handbook*. New York: McGraw-Hill, 1943, p. 51.

[3] F. W. Grover, *Inductance Calculations*, Princeton: Van Nostrand, 1946; reprinted by Dover Publications, 1962, pp. 17–47.

[4] H. A. Wheeler, "Simple inductance formulas for radio coils," *Proc. IRE*, vol. 16, pp. 1398–1400, 1928.

[5] H. E. Bryan, "Printed inductors and capacitors," *Tele-Tech & Electron. Ind.*, vol. 12, pp. 68–124, 1955.

[6] D. A. Daly, S. P. Knight, M. Caulton, and R. Ekholdt, "Lumped elements in microwave integrated circuits," *IEEE Trans. Microwave Theory Tech.*, vol. MTT-15, pp. 713–721, 1967.

[7] M. Caulton, B. Hershenov, S. P. Knight, and R. E. DeBrecht, "Status of lumped elements in microwave integrated circuits—Present and future," *IEEE Trans. Microwave Theory Tech.*, vol. MTT-19, pp. 588–599, 1971.

[8] C. S. Aitchison, R. Davies, I. D. Higgins, S. R. Longley, B. H. Newton, J. F. Wells, and J. C. Williams, "Lumped-circuit elements at microwave frequencies," *IEEE Trans. Microwave Theory Tech.*, vol. MTT-19, pp. 928–937, 1971.

[9] J. S. Joshi, J. R. Cockrill, and J. A. Turner, "Monolithic microwave gallium arsenide FET oscillators," *IEEE Trans. Electron Devices*, vol. ED-28, pp. 158–162, 1981.

[10] Y. C. Lim and R. A. Moore, "Properties of alternately charged coplanar parallel strips by conformal mapping," *IEEE Trans. Electron Devices*, vol. ED-15, pp. 173–180, 1968.

[11] R. S. Pengelly and D. C. Rickard, "Measurement and application of lumped elements up to *J*-band," in *Proc. 7th European Microwave Conf.* (Copenhagen), 1977.

[12] R. S. Pengelly, "Monolithic GaAs IC's tackle analog tasks," *Microwaves*, vol. 18, p. 56, July 1979.

[13] S. J. Haefner, "Alternating current of rectangular conductors," *Proc. IRE*, vol. 25, pp. 434–447, 1937.

[14] P. Waldow and I. Wolff, "Dual bounds variational formulation of skin effect problems," in *IEEE MTT-S Int. Microwave Symp. Dig.* (Las Vegas), 1987, pp. 333–336.

[15] R. A. Pucel, D. J. Massé, and C. P. Hartwig, "Losses in microstrip," *IEEE Trans. Microwave Theory Tech.*, vol. MTT-16, pp. 342–350, 1968; correction, vol. MTT-16, p. 1064, 1968.

[16] K. Meetz and W. L. Engl, *Elektromagnetische Felder*. Berlin, Heidelberg, New York: Springer, 1980, p. 234.

[17] C. Hentschel, "Konzentrierte Dünnfilmreaktanzen," Doctoral thesis, Technical University of Aachen, FRG, 1971.

[18] C. Hentschel, "Die Analyse von Schaltungen mit Dünnfilm-Spulen," *Arch. Elek. Übertragung.*, vol. 26, pp. 319–328, 1972.

[19] F. Ollendorff, *Berechnung magnetischer Felder*. Wien: Springer Verlag, 1952.

[20] R. L. Remke and G. A. Burdick, "Spiral inductors for hybrid and microwave applications," in *Proc. 24th Electron Components Conf.* (Washington, DC), May 1974, pp. 152–161.

[21] H. M. Greenhouse, "Design of planar rectangular microelectronic inductors," *IEEE Trans. Parts, Hybrids, and Packaging*, vol. PHP-10, pp. 101–109, June 1974.

[22] H. Katoh, "A lumped-element approach to microwave integrated circuits," *Electron. Commun. Japan*, vol. 56-B, pp. 713–721, 1967.

[23] D. Schieber, "On the inductance of printed spiral coils," *Arch. Elektrotech.*, vol. 68, pp. 155–159, 1985.

[24] D. M. Krafcsik and D. E. Dawson, "A closed-form expression for representing the distributed nature of the spiral inductor," in *1986 IEEE MTT-S Int. Microwave Symp. Dig.*, pp. 87–92.

[25] R. Garg and I. J. Bahl, "Characteristics of coupled microstriplines," *IEEE Trans. Microwave Theory Tech.*, vol. MTT-27, pp. 700–705, 1979.

[26] M. Kirschning and R. H. Jansen, "Accurate model for effective dielectric constant of microstrip with validity up to millimetre-wave frequencies," *Electron. Lett.*, vol. 18, pp. 272–273, 1982.

[27] W. O. Camp Jr., S. Tiwari, and D. Parson, "2–6 GHz monolithic microwave amplifier," in *1983 IEEE MTT-S Int. Microwave Symp. Dig.* (Boston), pp. 46–49.

[28] D. Cahana, "A new transmission line approach for designing spiral microstrip inductors for microwave integrated circuits," in *1983 IEEE MTT-S Int. Microwave Symp. Dig.* (Boston), pp. 245–247.

[29] I. Wolff and G. Kibuuka, "Computer models for MMIC capacitors and inductors," in *Proc. 14th European Microwave Conf.* (Liège), 1984, paper B 10.2.

[30] A. B. Dalby, "Interdigital microstrip circuit parameters using empirical formulas and simplified models," *IEEE Trans. Microwave Theory Tech.*, vol. MTT-27, pp. 744–752, 1979.

[31] M. Parisot, Y. Archambault, D. Pavlidis, and J. Margashack, "Highly accurate design of spiral inductors for MMIC's with small size and high cut-off frequency characteristics," in *1984 IEEE MTT-S Int. Microwave Symp. Dig.*, May 1984, pp. 106–111.

[32] G. I. Zysman and A. K. Johnson, "Coupled transmission line networks in an inhomogeneous dielectric medium," *IEEE Trans. Microwave Theory Tech.*, vol. MTT-17, pp. 753–758, 1969.

[33] V. A. Monaco and P. Tiberio, "Computer-aided analysis of microwave circuits," *IEEE Trans. Microwave Theory Tech.*, vol. MTT-22, pp. 249–263, 1974.

[34] M. Kirschning, "Entwicklung von Näherungsmodellen für den rechnergestützten Entwurf von hybriden und monolithischen Schaltungen in Mikrostreifenleitungstechnik," *Doctoral thesis*, University of Duisburg, FRG, 1984.

[35] R. H. Jansen and N. H. Koster, "Generalized least *p*-th optimization in the modelling of microwave transistors," *Arch. Elek. Übertragung.*, vol. 31, pp. 475–477, 1977.

[36] W. H. Chang, "Analytical IC metal-line capacitance formulas," *IEEE Trans. Microwave Theory Tech.*, vol. MTT-24, pp. 608–611, 1976.

[37] I. Wolff, *Einführung in die Mikrostrip-Leitungstechnik*. Aachen: Verlag H. Wolff, 1974/1978.
[38] G. D. Alley, "Interdigital capacitors and their application to lumped-element microwave integrated circuits," *IEEE Trans. Microwave Theory Tech.*, vol. MTT-18, pp. 1028–1033, 1970.
[39] J. L. Hobdell, "Optimization of interdigital capacitors," *IEEE Trans. Microwave Theory Tech.*, vol. MTT-27, pp. 788–791, 1972.
[40] R. Esfandiari, D. W. Maki, and M. Siracusa, "Design of interdigitated capacitors and their application to GaAs filters," *IEEE Trans. Microwave Theory Tech.*, vol. MTT-31, pp. 57–64, 1983.
[41] D. Kajfez, Z. Paunovic, and S. Pavlin, "Simplified design of Lange coupler," *IEEE Trans. Microwave Theory Tech.*, vol. MTT-26, pp. 806–808, 1978.
[42] R. E. DeBrecht, "Impedance measurement of microwave lumped elements from 1 to 12 GHz," *IEEE Trans. Microwave Theory Tech.*, vol. MTT-20, pp. 41–48, 1972.

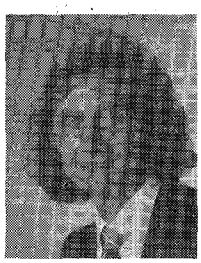

Ewald Pettenpaul was born in Porta Westfalica, Germany, in 1948. He received the Diplom-Physiker and Dr.-Ing. degrees in electrical engineering from the University of Hannover, Hannover, Germany, in 1974 and 1977, respectively.

In 1978, he joined the Development Department of Siemens Components Groups, Munich, Germany. His main research areas for nine years have been GaAs sensors, MESFET's, and IC's. Currently he is in charge of several development groups for GaAs devices.

Dr. Pettenpaul is the author or coauthor of numerous papers in the field of SIC and GaAs devices.

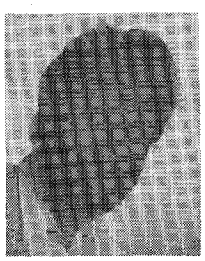

Hartmut Kapusta was born on August 1, 1948, in Walsum, Germany. He studied electrical engineering at the Technical University of Aachen, Germany, where he obtained the Dr.-Ing. degree in 1982.

In 1983 and 1984 he worked on MIC development at Philips, Eindhoven, The Netherlands. In 1984 he joined the Siemens Component Division, Munich, Germany, where he is currently CAD group leader of the GaAs MMIC development team.

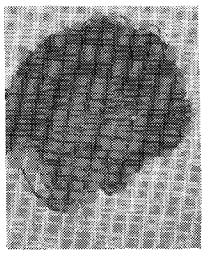

Andreas Weisgerber was born on October 21, 1963, in Saarwellingen, Germany. He studied electrical engineering at the Fachhochschule Koblenz, Germany, where he received the Dipl.-Ing. degree in 1986.

Since 1986 he has been with the Siemens Component Division, Munich, Germany, where he is currently a CAD group member of the GaAs MMIC development team.

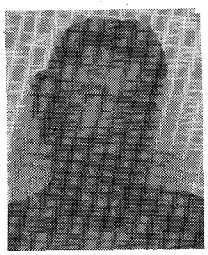

Heinrich Mampe was born on July 3, 1945, in Königsberg, Bavaria, Germany. He received the Dipl.Ing. degree in radio-frequency and microwave techniques from the Technical University of Munich, Germany, in 1973.

In 1974 he joined the Siemens AG, Munich, where he worked until 1980 in a Satellite Communication Group. Since 1980 he has been with the Siemens Components Division, where he is engaged in the design and measurement of small signal GaAs MMIC's for microwave applications.

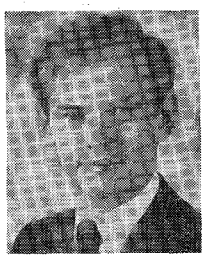

Jürgen Luginsland was born on February 4, 1958, in Emmerich, Germany. He studied electrical engineering from 1976 to 1981 at the Technical University of Aachen, Germany, where he obtained the Dr.-Ing. degree in 1985.

Since 1985 he has been with the Siemens Component Division, Munich, Germany, where he is currently a CAD group member of the GaAs MMIC development team.

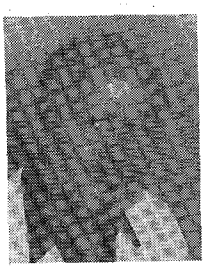

Ingo Wolff (M'75–SM'85) was born on September 27, 1938, in Köslin, Germany. He studied electrical engineering at the Technical University Aachen, Aachen, West Germany. In 1967 he obtained the Dr.-Ing. degree and in 1970 the Habilitation degree in high-frequency techniques from the Technical University Aachen.

Since 1974 he has been a Full Professor for electromagnetic field theory at the University of Duisburg, Duisburg, West Germany. His main research areas at the moment are numerical field analysis methods, modeling of planar hybrid and monolithic integrated microwave circuits, planar microwave antennas, and material parameter measurements at microwave and millimeter-wave frequencies.